# Tuning the magnetic anisotropy of single U atoms on MgO/Ag(001)

Wei Feng,[1,*,†] Mingming Fu,[2,*] Ping Yang,[1,*] Qiang Zhang,[1] Qunqing Hao,[1] Xiangfei Yang,[1] Yun Zhang,[1] Xiegang Zhu,[1] Shiyong Tan,[1] Zhenpeng Hu,[3] Qiuyun Chen,[1,‡] Qin Liu,[1,§] and Xinchun Lai[1]

[1]*Science and Technology on Surface Physics and Chemistry Laboratory, Mianyang, Sichuan 621908, China*

[2]*Department of Physics, Nanchang University, Nanchang, Jiangxi 330031, China*

[3]*School of Physics, Nankai University, Tianjin 300071, China*

(Received 23 August 2023; accepted 13 November 2023; published 7 December 2023)

Searching for single-atom systems with large magnetic anisotropy energies and tunable magnetic states is of vital importance for both fundamental research of magnetism at the atomic scale and realization of future spin-based quantum computation or information storage schemes. Single $5f$ electron based actinide atoms are potential candidates for inducing large magnetic anisotropy energies (MAEs), yet they have been much less studied as compared with $3d$ or $4f$ single-atom systems. Here we present the adsorptive, electronic, and magnetic properties of a single $5f$ electron based uranium atom on two-monolayer MgO/Ag(001) by combining scanning tunneling microscopy/spectroscopy (STM/STS) and density functional theory. Our results reveal that single U atoms spontaneously adsorb at the hollow sites of the MgO/Ag(001) surface and they can be controllably switched between the hollow and the O-top sites of MgO/Ag(001) via STM atom manipulation. Most importantly, single U atoms at the O-top sites reveal complex tunneling spectral features, including a symmetric dip at the Fermi energy, which is the manifestation of the existence of a relatively large $5f$-driven magnetic anisotropy energy, whereas single U atoms at the hollow sites exhibit a two-lobe subatomic structure stemming from the valence electron orbitals of U itself and show no signs related with magnetic anisotropy. This work proves that single $5f$ electron based U atoms can possess a considerable uniaxial magnetic anisotropy via adsorbing at the appropriate sites on the carefully chosen supporting surface, and their magnetic states can be tuned by atom manipulation techniques.

DOI: 10.1103/PhysRevB.108.245407

## I. INTRODUCTION

Magnetic atoms adsorbed on nonmagnetic surfaces provide important platforms for both deepening the understanding of fundamental aspects of magnetic quantum properties on the atomic scale and realizing the ultrahigh density information storage or quantum spin processing by individual atomic spins [1–5]. On one hand, the fabrications of stable and reliable atomic-scale spin-based devices require magnetic adatoms with a large magnetic anisotropy energy (MAE), which describes the tendency to maintain a stable orientation of the magnetic moment against random fluctuations over time [6–8]. On the other hand, seeking for a viable way to alter the adsorption positions as well as the magnetic states of the individual magnetic adatoms on substrates also plays a key role in the process of constructing spintronic devices atom by atom [9–11]. Thus, it is imperative to find suitable supported elements and supporting surfaces to guarantee a large MAE, and also feasible routes to manipulations of the magnetic anisotropies of these adatoms. Scanning tunneling microscopy (STM) has been proved as an effective tool for fabricating atomic-scale structures and studying the magnetic properties of individual atoms [1,4,5,11,12]. Until now, STM combined with other experimental techniques identified various single-atom systems with large MAE, such as individual atoms and clusters of Fe and Co on Pt(111) [6,13], individual Co atoms on MgO/Ag(100) [8], single Fe and Mn atoms on CuN/Cu(100) [7], single Ho atoms on Pt(111) [14] and MgO/Ag(100) [1,15,16], individual Fe atoms on MgO/Ag(100) [17], Gd atoms and dimers on Pt(111) and Cu(111) [18], and so on [4,5,12]. Large magnetic anisotropy is usually developed on those individual $3d$ or $4f$ electron based magnetic adatoms by the interplay between the crystal field, a large orbital moment, and strong spin-orbit coupling (SOC) interaction [6,8,16,17,19], and the special- or low-symmetry bonding geometry for those adatoms is also crucial for further enhancing the MAEs [8,14,17].

Apparently, the reported experimental studies in this field mainly focus on the MAEs and magnetic properties of single $3d$ transition-metal adatoms [4,6–8,12,13,17] and $4f$ rare-earth adatoms [1,4,12,14–16,18]. Theoretical studies also predict the existence of large MAEs in $4d$ or $5d$ transition-metal adatoms [19]. Except for these transition-metal and rare-earth adatoms, actinide atoms with unpaired $5f$ electrons are in principle promising candidates for building atomic-scale magnets, because $5f$ electrons exhibit an intermediate character between the relatively more itinerant $3d$ and relatively more localized $4f$ electrons, and $5f$ electron based

*These authors contributed equally to this work.
†Corresponding author: fengwei610@163.com
‡Corresponding author: chenqiuyun@caep.cn
§Corresponding author: liuqin493@163.com

 

elements have more extended valence orbitals and stronger spin-orbit coupling than $4f$ elements do, which may guarantee a large MAE. Indeed, slow magnetic relaxations were detected in some carefully designed actinide-based single-molecule magnets [20–22] and a large MAE up to 48 meV and long coherence time were predicted in a U atom substituting Al on $Al_2O_3(0001)$ by first-principles calculations and model analyses [23]. Yet, there is little direct experimental observation and evidence of the existence of MAE in single $5f$ electron based actinide adatoms. Among all the $5f$ electron based actinide elements, uranium is widely used in nuclear industry and nuclear engineering and provides a rich platform for both fundamental research and engineering application. However, the high chemical reactivity and the high evaporation temperature (∼2100 K) of U metal impose a challenge on constructing low-dimensional U-containing samples on the atomic scale. As a consequence, the properties of single U atoms have been rarely investigated by experimental methods. Until recently, individual U atoms adsorbed on conducting surfaces were prepared and then investigated by STM in our group [24,25]. The properties of single U adatoms exhibit rich diversity, including $5f$-driven Kondo resonance on multilayer graphene/6H-SiC(0001), $Cu_2N$/Cu(100), Bi(110) [25], and Ag(111) [24]; subatomic features on graphene/6H-SiC(0001), $Cu_2N$/Cu(100), and Bi(110) [25]; and intermetallic surface reactions on Cu(111) and Ag(111) at low substrate temperatures [24]. However, more work needs to be done regarding the observation of experimental signs related with the $5f$ electron induced magnetic anisotropies in these systems. Further exploration of single U atoms adsorbed on various substrates is crucial for verifying the possibility of inducing MAE by $5f$ electron based atoms.

Here we report the observation of magnetic anisotropy revealed by the inelastic tunneling spectroscopies (IETSs) in single U atoms and the successful manipulation of the magnetic states of single U atoms by STM. Our STM observations combined with first-principles calculations show that the hollow site of the 2 ML MgO/Ag(001) surface is the spontaneous and energetically most favorable adsorption site for a U atom. Meanwhile, a U atom can be controllably switched from the hollow site to the O-top site and vice versa via STM atom manipulation techniques. Single U atoms on the O-top sites show complex features in the tunneling differential conductance ($dI/dV$) spectra, including a symmetric dip located at the Fermi energy ($E_F$); a peak and a hump, respectively located within the negative and positive sample biases. While the peak and hump originate from the resonance tunneling via the discrete atomic orbitals of U adatom in the double-barrier tunnel junction (DBTJ) [26–28] formed by the tip–vacuum layer–U adatom–MgO–Ag(001), the symmetric dip at $E_F$ is attributed to the spin-flip excitation with an excitation energy $E_{sf}$ of about 7.7 meV, which is induced by an out of plane magnetic anisotropy confirmed by both theoretical calculations and experimental characteristics. In contrast, a U atom at the hollow site exhibits a two-lobe subatomic structure, arising from the *sdf* suborbitals of U itself, in the $dI/dV$ maps, but it does not reveal any signatures relevant with MAE. These results signify that a switching of the MAE and magnetic state of the U atom is realized via repositioning it between the hollow and O-top sites on MgO(001)/Ag(001). Our study corroborates that single $5f$ electron based atoms can exhibit a detectable MAE through adsorbing on an appropriate supporting surface, and the atomic coordination and bonding geometry with the supporting surface determined by the specific adsorption configuration are vital for the creation of a considerable MAE.

## II. EXPERIMENTS AND METHODS

The preparation of the Ag(001) substrate and growth of ultrathin MgO films were carried out in an ultrahigh-vacuum (UHV) chamber with a base pressure below $8 \times 10^{-11}$ mbar. Ag(001) single crystal was cleaned by repeated cycles of $Ar^+$ sputtering and annealing to ∼620 K. We grew 2 ML MgO(001) films on a clean Ag(001) surface by depositing Mg under an oxygen pressure of $8 \times 10^{-7}$ mbar for 3–4 min while keeping the Ag(001) substrate at 470 K. To avoid oxidation and contamination of the highly reactive uranium, its deposition and the following STM measurements were performed in another UHV chamber with a base pressure greater than $1.5 \times 10^{-11}$ mbar. U metal with a purity of 99.9% was degassed and purified by a procedure presented in Ref. [24] before deposition. Then a small amount of U atoms were deposited onto 2 ML MgO film grown on Ag(001) by keeping the substrate at 7 K. All the measurements were performed by utilizing a commercial low-temperature STM operated at 4.2 K. Clean tungsten tips were used after $Ar^+$ sputtering and after being treated on a clean Cu(111) surface. The differential tunneling spectra ($dI/dV$) were recorded through a standard lock-in technique with a modulation frequency of 731 Hz and a rms modulation amplitude of $V_{mod} = 4$ mV.

DFT calculations were carried out using the Vienna *Ab initio* Simulation Package (VASP) [29]. Within the projector augmented wave (PAW) [30] framework, the plane-wave cutoff energy was set to be 400 eV. The exchange-correlation functional was treated within the Perdew-Burke-Ernzerhof (PBE) [31] version of generalized gradient approximation (GGA). Our periodic slab model is a $3 \times 3 \times 1$ supercell consisting of two Ag(001) layers and two layers of MgO(001) whose O atoms sit above the Ag atoms. To be consistent with the underlying Ag lattice, the in-plane lattice parameter of MgO was compressed by 2%. A vacuum layer of 15 Å was added towards the $z$ direction to eliminate the interactions between the neighboring slabs. During geometric optimization, we fixed the bottom two Ag layers and relaxed the other atoms fully until the residual atomic force on each atoms was smaller than 0.02 eV/Å. The magnetic anisotropy energy (MAE) was calculated by including spin-orbit coupling (SOC), and here the $k$-point mesh and energy convergence criterion were raised to $5 \times 5 \times 1$ and $1 \times 10^{-6}$ eV, respectively. The GGA+$U$ method was adopted to deal with the on-site Coulomb interaction between the $5f$ electrons in uranium [32,33]. The effect of varying the Hubbard $U$ value will be discussed later and is also shown in the Supplemental Material (Figs. S6 and S7 [34]; this includes Refs. [26–28,35–37]).

## III. RESULTS AND DISCUSSION

Figure 1(a) shows a typical topographic image of MgO film (or island) grown on Ag(001). Surface defects appearing

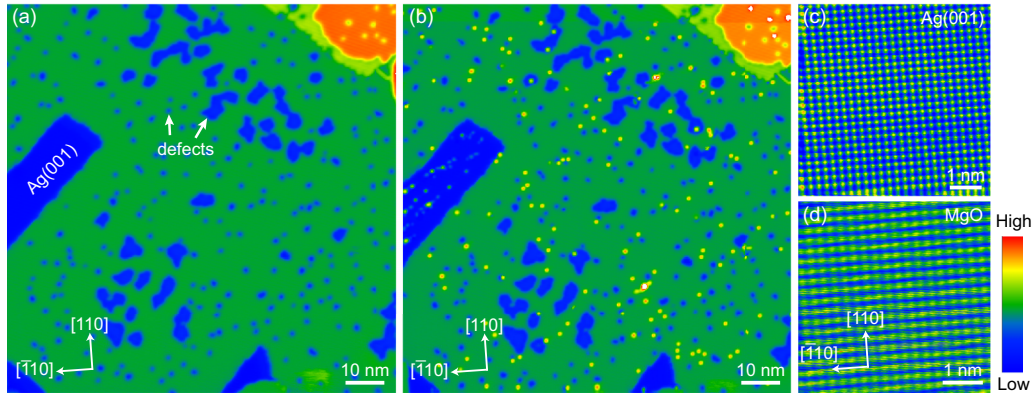


FIG. 1. U atoms on MgO/Ag(001) surface. STM topography of MgO/Ag(001) surface (a) before and (b) after the deposition of a small amount of U atoms ($V_b = 1.0$ V, $I = 100$ pA). White arrows indicate two examples of surface defects on the MgO film. Atomically resolved STM image of (c) clean Ag(001) surface ($V_b = 2$ mV, $I = 1.6$ nA) and (d) 2 ML MgO grown on Ag(001) ($V_b = 4$ mV, $I = 15.7$ nA).

as irregular depressions are commonly observed on the MgO films [35]. From Figs. 1(c) and 1(d), the surface atoms of MgO and Ag(001) are arranged in the same direction and the MgO film has a lattice constant of 2.94 Å. This value is very close to but a little bit smaller than $\sqrt{2}/2a_0 = 3.0$ Å, where $a_0 = 4.25$ Å is the lattice constant of bulk MgO [38]. These results corroborate that the grown MgO surface is the (001) plane and only one type of element, i.e., either Mg or O, is imaged by STM. Since *ab initio* calculations indicate that oxygen atoms have the highest density of electrons on the MgO(001) plane [39], the imaged atoms in Fig. 1(d) should be oxygen. The slight shrinkage of the STM-measured surface lattice constant (2.94 Å) on MgO/Ag(001) films compared to their bulk counterpart (3.00 Å) originates from the contraction of the grown MgO films caused by the 2% lattice mismatch between the Ag(001) substrates ($a_0 = 4.16$ Å) and bulk MgO. Furthermore, through carefully comparing the height profile of the MgO film measured under low biases with that taken above the energy level of the MgO(001) surface state (see Sec. SM I of the Supplemental Material [34]), we can determine that the thickness of the MgO film is two monolayers. After the deposition of U atoms, spherical protrusions with almost uniform heights and diameters are randomly distributed on the clean region of MgO/Ag(001) as shown in Fig. 1(b). The apparent sizes of these protrusions [also see Figs. 2(a)–2(d)] are comparable with those of single U atoms adsorbed on graphene/6H-SiC(0001), $Cu_2N$/Cu(100) [25], and transition-metal surfaces [24]. Therefore we can confirm that most spherical protrusions with uniform height are single U atoms rather than U clusters.

The uniform heights and diameters of U adatoms on MgO/Ag(001) imply that they spontaneously adsorb at the equivalent sites, which should be the most energetically stable adsorption sites for U. Intriguingly, we find these single U atoms can be controllably and reversibly repositioned among the spontaneous adsorption sites and a different kind of adsorption site on MgO(001) by STM atom manipulation. Figure 2(a) shows a small-scale topographic image including five U atoms on MgO/Ag(001) and one impurity atom with relatively lower apparent height. The impurity atom can act as a hallmark in the following manipulation operations. Via using a STM lateral manipulation method [40,41], we pushed two U atoms to a different kind of adsorption site [the white arrows mark the pushing direction in Fig. 2(a)], resulting in obvious enlargement of the apparent size as shown in Fig. 2(b). The measured height profiles [Fig. 2(d)] indicate the apparent sizes of these two U atoms are ~0.08 nm higher and 0.1 nm wider than before. Through applying 0.3 V voltage pulses, these two U atoms were switched back to their initial adsorption configurations [see Fig. 2(c)]. To figure out these adsorption configurations, we performed first-principles calculations in the framework of DFT, and four high-symmetry binding sites on MgO(001), including O-top, Mg-top, hollow,

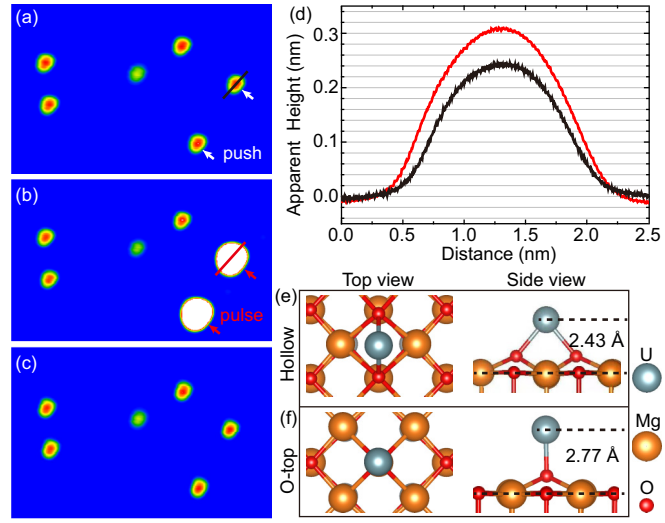


FIG. 2. Switching the adsorption configurations of single U atoms on MgO by STM atom manipulations. (a)–(c) A series of STM images showing the process of pushing two individual U atoms [the white arrows mark the pushing direction in panels (a)] from the hollow sites to the O-top sites by a STM lateral manipulation method [40,41] and then moving them back to the hollow sites by applying voltage pulses ($V_b = 0.1$ V, $I = 200$ pA). (d) Comparison of the height profiles measured across a U atom before [black line in panel (a)] and after [red line in panel (b)] the lateral manipulation. DFT calculated atomic structure of a U atom adsorbed (e) at hollow site and (f) atop an O atom of 2 ML MgO/Ag(001). Gray, red, and orange balls, respectively, represent U, O, and Mg atoms.

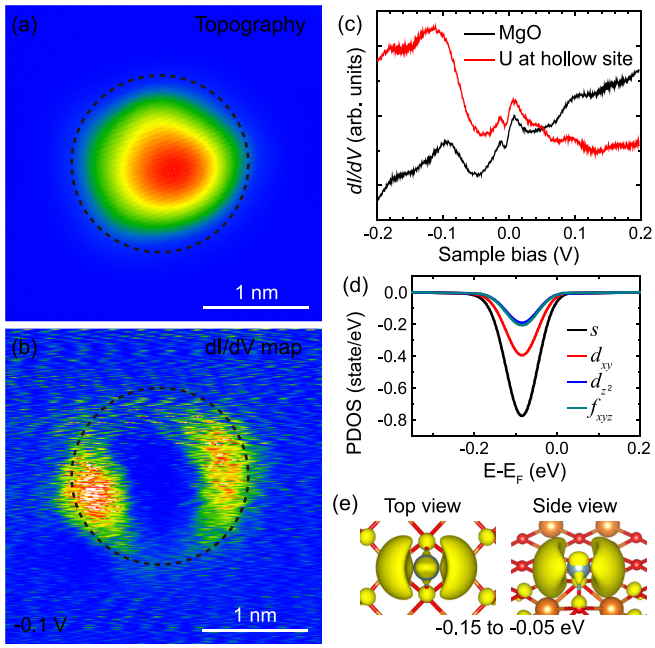


FIG. 3. Subatomic structure of single U atom adsorbed at the hollow site of MgO/Ag(001) observed by STM. (a) Topographic image and (b) $dI/dV$ map of an isolated U atom adsorbed at the hollow site of 2 ML MgO film on Ag(001) ($V_b = -0.1$ V, $I$=400 pA). (c) Comparison between typical $dI/dV$ spectra taken on clean area of MgO surface and that taken above a single U atom adsorbed at the hollow site of MgO. (d) Calculated PDOS of a single U adatom adsorbed at the hollow site of MgO. (e) Isosurface of charge density around a single U atom at the hollow site of MgO in the energy range of $-0.15$ to $-0.05$ eV. The isosurface value is taken as $1.5 \times 10^{-3}\, e\,\text{Å}^{-3}$. Red and orange balls represent O and Mg atoms, respectively. The results shown correspond to $U = 1$ eV (see Sec. SM IV in the Supplemental Material [34]).

and Mg-O bridge sites, were considered. During geometry optimization, the U atom on the hollow site stretches out two neighboring O atoms as shown in Fig. 2(e). The U atom on the Mg-top or bridge site transfers to the hollow site and forms the same structure. On the O-top site, the U atom can remain stable after pulling out the O underneath [Fig. 2(f)], and it is about 0.29 eV higher in energy than on the hollow site. As shown by the side view of the structural models in Figs. 2(e) and 2(f), the height of the U atom on the O-top site is 0.34 Å higher than that on the hollow site. The increased height naturally leads to a larger apparent size in the STM constant current image. Based on these results, we confirm that single U atoms spontaneously adsorb on the hollow sites after deposition, and they migrate to the neighboring O-top sites after STM lateral manipulations and hence appear larger in the topographic images.

Figure 3(a) shows the topographic image of an individual U atom adsorbed at the hollow site of MgO(001), and its characteristic $dI/dV$ spectrum together with the spectrum on bare MgO are shown in Fig. 3(c). Several peak features observed in the U spectrum are not the intrinsic features that arose due to the U atom itself. Instead, these features may stem from the specific density of states of either the STM tip or the MgO/Ag(001) substrate, since the same features were also detected on the bare MgO surface. Considering that the MgO layer has a large intrinsic insulating gap below 1.7 eV [35,36] and Ag(001) is metallic and does not have any surface states around $E_F$, these peak features should originate from the STM tip. It is noteworthy that the $dI/dV$ signal of the U atom displays a significant increase within the negative bias range. Via recording the spectra by other different STM tips (see Figs. S3(a) and S3(d) [34]), we confirm that the increase of the $dI/dV$ signal is directly related with the U atom, instead of any tip states. Meanwhile, the $dI/dV$ map of the U atom at the hollow site [Fig. 3(b)] taken at $-0.1$ V shows a two-lobe structure. The charge distribution calculated by the GGA+$U$ method via choosing Hubbard $U = 1$ eV can precisely reproduce the measured two-lobe structure in the $dI/dV$ map [Fig. 3(b)], as shown in Fig. 3(e). Our calculations indicate that Mg atoms nearly show no density of states in the energy range of $-0.15$to $-0.05$ eV and O atoms also display very small spherical isosurfaces of a charge density of $1.5 \times 10^{-3}\, e\,\text{Å}^{-3}$, which do not overlap with the electronic states of the U atom. As shown in Fig. 3(d), there exist only the $s$, $d_{xy}$, $d_{z^2}$, and $f_{xyz}$ states from the U atom itself in this energy range. Consequently, we can confirm that the two-lobe structure arises from the superposition of U's valence states. There are few reports of such distinct observations of subatomic structures in other single-atom systems, except for our previous study of single U atoms on other metal or semiconducting surfaces [25]. The significant enhancement of the $dI/dV$ signals within the negative biases on the U atom also results from the much larger occupied density of states in these U suborbitals compared with those on a bare MgO(001) surface.

In contrast, U atoms adsorbed at the O-top site of MgO display rich tunneling spectral features. Figures 4(a) and 4(b) show the $dI/dV$ spectra measured at different sites [marked by the black dots in the inset of Fig. 4(a)] above an isolated U adatom at the O-top site as well as on bare MgO. The spectra on U adatoms are dominated by three typical features: a dip located at the Fermi energy ($E_F$), a hump (in other words, a broadened peak) [indicated by the arrows in Fig. 4(a)] located at positive biases, and a peak [indicated by the arrows in Fig. 4(b)] located at negative biases, whereas the $dI/dV$ spectra recorded on bare MgO by the same STM tip do not show any obvious features. This confirms that these observed spectral features indeed stem from the U adatom rather than the special tip states. When the STM tip is moved outwards from the atom center, the hump or peak structures, respectively, shift towards higher or lower energies. The shifting behavior of a pair of peaks upon leaving the atom center is a typical manifestation of resonance tunneling through a double-barrier tunnel junction (DBTJ) [26–28]. Indeed, the STM tip, vacuum layer, U adatom, MgO layer, and Ag(001) substrate together can constitute a DBTJ, among which the vacuum barrier and the insulating MgO layer act as the two tunneling barriers. In this case, if an appropriate bias voltage is applied, electrons can pass through the DBTJ via discrete atomic orbitals (DAOs) of the U adatom, which will cause a sudden current increase, usually appearing as a peak in the $dI/dV$ curve [26–28]. Through carefully analyzing the behaviors of the two spectral features (see the detailed discussions in Sec. SM III [34]), we conclude that the hump or peak are

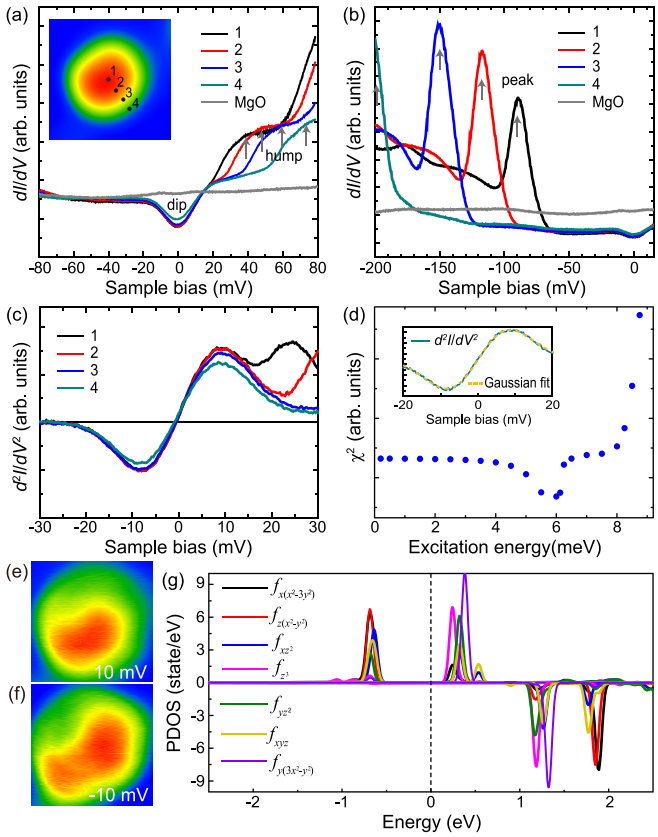


FIG. 4. Uniaxial magnetic anisotropy effect in a single U atom at the O-top site and single electron tunneling in the DBTJ formed by the tip–vacuum layer–U adatom–MgO–Ag(001). $dI/dV$ spectra (a) around $E_F$ and (b) focusing on negative biases taken at different positions [marked by the black dots in the inset of panel (a)] above an individual U atom at the O-top site. Inset in panel (a) STM topography of the single U atom at the O-top site. For comparison, the typical spectra of the bare MgO/Ag(001) surface are shown as gray curves in panels (a), (b). The hump and the peak features in each spectrum are indicated by colored peaks in panels (a), (b). (c) Inelastic tunneling spectra ($d^2I/dV^2$) around $E_F$ taken at the same positions marked by the black dots in the inset of panel (a) ($V_b = -80$ mV, $I$=600 pA). (d) The mean square deviation ($\chi^2$) as a function of excitation energy, i.e., peak position. $\chi^2$ is obtained in the Gaussian fitting of the dip-peak structure in the $d^2I/dV^2$ spectrum of a U atom at the O-top site. Inset in (d) shows an example of Gaussian fit (represented by the yellow dashed line) to the $d^2I/dV^2$ spectra of the U atom. (e), (f) $dI/dV$ maps of the U atom at the O-top site taken at (e) $V_b =$ 10 mV and (f) $V_b = -10$ mV ($I = 600$ pA). (g) Calculated $5f$ orbital decomposed DOS of a U atom at the O-top site.

induced by resonance tunneling through the vacuum barrier to the lowest unoccupied discrete atomic orbital (LUDAO) of U or from the highest occupied discrete atomic orbital (HODAO) in the DBTJ, respectively.

In sharp contrast with the shifting behavior of the hump and peak, the amplitude and energy position of the dip feature remains almost unchanged upon leaving the U atom center as shown in Fig. 4(a). In particular, the dip feature is almost symmetric with respect to $E_F$. To further verify its symmetry, we numerically differentiate the $dI/dV$ spectra and smooth them to obtain the curves in Fig. 4(c). The $d^2I/dV^2$ curves indeed reveal a local dip-peak structure with the local minimum and maximum symmetrically located below and above $E_F$. The differential conductance maps taken at $\pm 10$ meV [see Figs. 4(e) and 4(f)] indicate that the energetically symmetric dip feature in $dI/dV$ is nearly homogeneously distributed inside the U adatom. Several possibilities, including a Kondo effect, atomic vibrations, or spin-flip excitations, can produce a dip feature around $E_F$ in the $dI/dV$ spectrum. The Kondo resonance usually behaves as an asymmetric line shape in the $dI/dV$ curve and it can produce a symmetric dip feature only when the probability of tunneling into the continuum conduction bands of the host substrate is much larger than that of tunneling into the Kondo resonance state [42]. Generally speaking, the energy position of the Kondo resonance dip is close to but not exactly coincident with $E_F$ and the amplitude of the Kondo dip distinctly decreases upon leaving the magnetic atom center, as observed in single U atoms adsorbed on graphene/6H-SiC(0001), $Cu_2N$/Cu(100), and Bi(110) [25]. Although the possibility of a Kondo effect cannot be fully excluded, both the symmetric line shape and the unchanged amplitude of the dip feature suggest that the Kondo effect is less likely to be the cause of the observed dip. To detect atomic vibrations, an extremely high signal to noise ratio is needed for the STM measurements. However, the vibration noise of our STM in the $z$ direction, i.e., normal direction of sample surface, is about 4 pm. Under this condition, our STM cannot probe the atomic vibrations. So the dip feature is more likely to be attributed to the magnetic spin-flip excitation driven by the inelastic electron tunneling which transfers energy and angular momentum to the U adatom. Nevertheless, to fully confirm whether the dip arises from magnetic excitation, a stronger evidence would be to observe a shift of the excitation energy under a magnetic field. It is necessary to perform more experiments under magnetic fields to further verify our point in the future. Even so, such a magnetic excitation manifested as a symmetric dip in $dI/dV$ or a dip-peak structure in the $d^2I/dV^2$ spectra has been observed in many other single magnetic atom systems [13,14,18,43]. However, even giant magnetic anisotropy or magnetic remanence has been identified for single $3d$ transition-metal (Co, Fe) atoms [8,17] or $4f$ rare-earth (Ho) atoms adsorbed at the O-top site on MgO/Ag(100) [1,15,16], experimental indication of the magnetic excitations of single $5f$ electron based actinide atoms reported here.

The spin-flip excitation energy $E_{sf}$ can be determined from the Gaussian fitting of the dip-peak structure [e.g., the fitting curve in the inset of Fig. 4(d)]. Figure 4(d) shows the mean square deviation $\chi^2$ as a function of peak position obtained from the fitting of the $d^2I/dV^2$ spectrum of a U atom at the O-top site. A clear minimum appears at 6 meV. We repeated this operation for several different single U atoms, and all of them yield a distinct minimum of $\chi^2$ at similar energies, leading to a mean value of $6.1 \pm 0.1$ meV. Naturally, this energy, at which the minimum of $\chi^2$ appears, can be taken as the excitation energy $E_{sf}$. However, it is worth noting that the instrumental broadening can impose a dramatic effect on the measured inelastic spectra. According to the studies of Balashov *et al.*, when the dip-peak distance becomes comparable to or smaller than the instrumental broadening, the peaks appear at positions increasingly deviated from the real

excitation energy [12,44]. On the contrary, if the dip-peak distance is larger than the instrumental broadening, the peak positions appear essentially unshifted [12,44]. In our current work, the instrumental broadening is mainly contributed by three factors: thermal broadening ($5.4\,k_BT$), bias modulation amplitude ($1.7\,\mathrm{eV_{mod}}$), and the loss of energy resolution ($W_{\mathrm{smooth}} = 1.95$ meV) caused by smoothing the $d^2I/dV^2$. Therefore, the total instrumental broadening is determined by $W_{\mathrm{instrum}} = [W^2_{\mathrm{smooth}} + (5.4k_BT)^2 + (1.7\,\mathrm{eV_{mod}})^2]^{1/2}$, yielding a value of 7.3 meV. Obviously, the dip-peak distance ($12.2 \pm 0.2$ meV) is larger than the instrumental broadening. Therefore we can conclude that the peak and dip positions are essentially unshifted in our experiments. Even so, it is important to further check the excitation energy by using a smaller modulation voltage or performing the measurements at lower temperatures after we update our instrument in the future.

The average full width at half maximum (FHWM) of the dip-peak structures on several single U atoms at the O-top sites is determined as $15.8 \pm 1.2$ meV based on the criterion of minimum $\chi^2$ in Gaussian fitting. The lifetime $\tau$ of the magnetic excitation can be estimated by the uncertainty principle $\tau W \geqslant \hbar/2$, where $W$ is the intrinsic width of the dip-peak structure [18]. The relation between the measured FHWM, the instrumental broadening $W_{\mathrm{instrum}}$, and the intrinsic width $W$ is given by $\mathrm{FHWM} = (W^2 + W^2_{\mathrm{instrum}})^{1/2}$ [45]. Based on these relations, we can obtain that the intrinsic width $W$ is 14 meV and the excitation lifetime $\tau$ of the U atom at the O-top site is about 24 fs. The height of the dip in the $dI/dV$ spectrum reveals that about 42% of the tunneling electrons participate in the spin-flip excitation, leading to a time of 0.63 ns between consecutive excitation events for $I = 600$ pA. This time is four orders of magnitude longer than the magnetic excitation lifetime. Therefore, there are no consecutive multilevel excitations and only excitations from the ground state are probed in our experiments.

The relationship between the classical MAE and the spin-flip excitation energy $E_{sf}$ can be estimated by this formula: $\mathrm{MAE} = E_{sf} \times J^2/(2J-1)$ [13,18], where $J$ is total angular momentum. Since the orbital angular momentum is prone to decrease or quench when the atom adsorbs on the substrate, the $J$ value of the U atom should be smaller than 6, i.e., the $J$ value of a free U atom. Because the experimentally determined $E_{sf}$ of the U atom at the O-top site is ~6.1 meV, the corresponding MAE should be smaller than 20 meV. Since SOC is the prerequisite to inspire magnetic anisotropy, we included the SOC effect and adopted the GGA+$U$ method to compute the MAE of the U atom at the O-top site. Figures S6(a) and S6(b) [34] show that the value of Hubbard $U$ has a dramatic effect on the calculated MAE. The MAEs of both sites calculated by GGA are negative, corresponding to an in-plane easy magnetic axis. After including on-site Coulomb interaction, the MAE changes drastically and the easy magnetization axis switches to the $z$ axis. Therefore, to match the measured value of $E_{sf}$ and the easy magnetization axis, a Hubbard $U$ value around 0.5 eV is a reasonable result for a U atom adsorbed at the O-top site. To obtain further understanding of the origin of the perpendicular MAE, we consider the second-order perturbative contribution of spin-orbit coupling (SOC) to MAE depending on the atomic site and the spin transition process [10,46,47]. The orbital-decomposed densities of $5f$ states of a U atom at the O-top site with a Hubbard $U = 0.5$ eV were calculated and are shown in Fig. 4(g). Since the minority-spin occupied states are almost zero, the main contributions of MAE arise from the spin-conservation term $\Delta E^U_{\uparrow\Rightarrow\uparrow}$ and the spin-flip term $\Delta E^U_{\uparrow\Rightarrow\downarrow}$. To estimate $\Delta E^U_{\sigma\Rightarrow\sigma'}$, the angular momentum matrix elements are considered. It is found that the minority-spin unoccupied U-$f_{x(x^2-3y^2)}$ and U-$f_{z(x^2-y^2)}$ states are much larger than the majority-spin unoccupied U-$f_{x(x^2-3y^2)}$ and U-$f_{z(x^2-y^2)}$ states, as shown by the black and red curves. Consequently, the spin-flip term $\Delta E^U_{\uparrow\Rightarrow\downarrow}$ of $\langle yz^2|L_x|x(x^2-3y^2)\rangle$, $\langle xyz|L_x|x(x^2-3y^2)\rangle$, and $\langle yz^2|L_x|z(x^2-y^2)\rangle$ make a positive contribution to MAE, while the spin-flip term $\Delta E^U_{\uparrow\Rightarrow\uparrow}$ of $\langle y(3x^2-y^2)|L_x|x(x^2-3y^2)\rangle$ and $\langle xyz|L_z|z(x^2-y^2)\rangle$ makes the primary negative contribution. Furthermore, the positive contribution and negative contribution to MAE from other angular momentum matrices are almost equal due to the similar majority-spin unoccupied states and minority-spin unoccupied states. Meanwhile, the contributions from the $6d$ states of U are negligible. To sum up, the MAE contributed from all nonvanishing angular momentum matrix elements is positive, resulting in an effective $5f$-driven out of plane magnetic anisotropy.

In contrast to the distinct spectral structure driven by the magnetic excitations for a U atom at the O-top site, the U atom at the hollow site does not show any spectral features related with the spin-flip excitation at $E_F$ [see Fig. 3(c)], suggesting the absence of magnetic excitation or a negligible excitation magnitude, which is hard to detect under the current experimental condition. By considering the effective instrumental broadening, its MAE should be smaller than 4.2 meV. According to Figs. S6(b) and S7 [34], the calculated MAE at a Hubbard $U \leqslant 1$ eV agrees well with the experimental result for the U atom at the hollow site. By considering the second-order perturbative contribution of SOC to MAE from our calculations, the out of plane contribution and in-plane contribution to MAE are comparable with each other and hence being offset, leading to a very small total MAE for a U atom at the hollow site. The large discrepancy between the MAE of a U atom at the O-top and hollow site indicates that the specific adsorption configuration (or site) of the magnetic atom on the supporting surface plays an important role in the formation of magnetic anisotropy. Different adsorption configurations result in significantly different coordination numbers and bonding geometries. The distinct reducing of the coordination number (from 4 to 1) for the U atom switching from the hollow site to the O-top site is probably one of the decisive factors for inducing a visible MAE. It is noteworthy that the XMCD (x-ray magnetic circular dichroism) study of the $3d$ cobalt nanoparticles also confirm that the MAE depends on the single-atom coordination and MAE decreases strongly with increasing Co coordination, which is in line with our result [6].

Another important factor for inducing a visible MAE is choosing an appropriate supporting surface. Previously, we have systematically studied single U atoms

adsorbed on various surfaces, ranging from metal [Cu(111), Ag(111), Au(111), Ru(0001), Bi(110)] to semiconducting [graphene/6H-SiC(0001)] to insulating [$Cu_2N$/Cu(100)] surfaces [25], yet none of them show any experimental signatures connected with magnetic anisotropy. Previous studies on a $4f$ adatom performed by Donati *et al.* indicate that choosing a proper tunnel barrier to decouple the spin of a magnetic atom from the underlying metal is crucial for the realization of a large atomic MAE [16]. Also, the MgO thin film has been demonstrated as a useful decoupling layer for the $3d$- [8,17] and $4f$- [1,15,16] as well as the $5f$-U single atoms. The MgO layer is insulating and hence can provide a large gap to somehow isolate the thermal bath of the substrate electrons. However, having only an insulating layer is not enough to guarantee a large MAE; this is demonstrated by the absence of magnetic anisotropy in the U atom (with a coordination number of 4) on $Cu_2N$/Cu(100), where the $Cu_2N$ thin film is also insulating [25]. Another important characteristic making the MgO thin film special is that it provides a special adsorption site, i.e., the O-top site, which allows the lowest coordination number (of 1) for the surface magnetic adatom, ensuring a large MAE or even a stable symmetry-protected magnetic ground state [16].

## IV. CONCLUSION

To summarize, our STM and theoretical studies provide an overall picture about the adsorptions, and electronic and magnetic properties of a single $5f$ electron based uranium atom on a 2 ML MgO/Ag(001) surface and present a direct observation of a considerable MAE in single U atoms. The U atom at the hollow site of MgO displays a two-lobe subatomic structure, arising from the U's $s$, $d$, and $f$ states, in the $dI/dV$ map and it does not exhibit any experimental signatures of magnetic anisotropy. In contrast, the U atom at the O-top site reveals complex spectral features, including two features related with resonance tunneling through U's atomic orbitals in the DBTJ and a symmetric dip at $E_F$ induced by the inelastic spin-flip excitation, which reflects a nearly perpendicular magnetic anisotropy under the presence of SOC and a proper correlation effect. The notable difference between the MAEs of U at the O-top and hollow sites emphasizes the importance of the specific atomic bonding geometry and the coordination number of the magnetic adatom on the supporting surface for attaining a large MAE. The capability of repositioning the U atom between the hollow and O-top site by STM atom manipulation techniques thus equivalently enables us to tune the individual atomic spins on the metal-supported insulating thin films, which is a crucial step towards building nanoscale or atomic-scale spintronic devices. Our work offers inspiration of how to create an atomic MAE via choosing proper supporting substrates for individual $5f$ electron based adatoms and thus provides an opportunity to investigate the possibility of constructing nanoscale or atomic-scale $5f$ electron based spintronic devices or quantum memory in the future.

## ACKNOWLEDGMENTS

This work was supported by the National Science Foundation of China (Grants No. 12122409, No. 11974319, and No. 11904335) and the National Key Research and Development Program of China (Grants No. 2022YFA1402201 and No. 2021YFA1601101).

[1] F. D. Natterer, K. Yang, W. Paul, P. Willke, T. Choi, T. Greber, A. J. Heinrich, and C. P. Lutz, Reading and writing single-atom magnets, Nature (London) **543**, 226 (2017).

[2] A. A. Khajetoorians and J. Wiebe, Hitting the limit of magnetic anisotropy, Science **344**, 976 (2014).

[3] A. A. Khajetoorians and A. J. Heinrich, Toward single-atom memory, Science **352**, 296 (2016).

[4] T. Choi, Studies of single atom magnets via scanning tunneling microscopy, J. Magn. Magn. Mater. **481**, 150 (2019).

[5] M. Ternes, Probing magnetic excitations and correlations in single and coupled spin systems with scanning tunneling spectroscopy, Prog. Surf. Sci. **92**, 83 (2017).

[6] P. Gambardella, S. Rusponi, M. Veronese, S. S. Dhesi, C. Grazioli, A. Dallmeyer, I. Cabria, R. Zeller, P. H. Dederichs, K. Kern, C. Carbone, and H. Brune, Giant magnetic anisotropy of single cobalt atoms and nanoparticles, Science **300**, 1130 (2003).

[7] C. F. Hirjibehedin, C. Y. Lin, A. F. Otte, M. Ternes, C. P. Lutz, B. A. Jones, and A. J. Heinrich, Large magnetic anisotropy of a single atomic spin embedded in a surface molecular network, Science **317**, 1199 (2007).

[8] I. G. Rau, S. Baumann, S. Rusponi, F. Donati, S. Stepanow, L. Gragnaniello, J. Dreiser, C. Piamonteze, F. Nolting, S. Gangopadhyay, O. R. Albertini, R. M. Macfarlane, C. P. Lutz, B. A. Jones, P. Gambardella, A. J. Heinrich, and H. Brune, Reaching the magnetic anisotropy limit of a $3d$ metal atom, Science **344**, 988 (2014).

[9] M. Tanveer, J. Dorantes-Davila, and G. M. Pastor, Reversible electric-field manipulation of the adsorption morphology and magnetic anisotropy of small Fe and Co clusters on graphene, Phys. Rev. B **96**, 224413 (2017).

[10] M. Fu, W. Tang, Y. Wu, C. Ke, F. Guo, C. Zhang, W. Yang, Z. Wu, and J. Kang, Manipulation of perpendicular magnetic anisotropy of single Fe atom adsorbed graphene via MgO(111) substrate, J. Phys. D: Appl. Phys. **51**, 205001 (2018).

[11] A. A. Khajetoorians, J. Wiebe, B. Chilian, and R. Wiesendanger, Realizing all-spin-based logic operations atom by atom, Science **332**, 1062 (2011).

[12] T. Balashov, T. Miyamachi, T. Schuh, T. Maerkl, C. Bresch, and W. Wulthekel, Dynamic magnetic excitations in $3d$ and $4f$ atoms and clusters, Surf. Sci. **630**, 331 (2014).

[13] T. Balashov, T. Schuh, A. F. Takács, A. Ernst, S. Ostanin, J. Henk, I. Mertig, P. Bruno, T. Miyamachi, S. Suga, and W. Wulfhekel, Magnetic anisotropy and magnetization dynamics of individual atoms and clusters of Fe and Co on Pt(111), Phys. Rev. Lett. **102**, 257203 (2009).

[14] T. Miyamachi, T. Schuh, T. Markl, C. Bresch, T. Balashov, A. Stohr, C. Karlewski, S. Andre, M. Marthaler, M. Hoffmann,

M. Geilhufe, S. Ostanin, W. Hergert, I. Mertig, G. Schon, A. Ernst, and W. Wulfhekel, Stabilizing the magnetic moment of single holmium atoms by symmetry, Nature (London) **503**, 242 (2013).

[15] F. D. Natterer, F. Donati, F. Patthey, and H. Brune, Thermal and magnetic-field stability of holmium single-atom magnets, Phys. Rev. Lett. **121**, 027201 (2018).

[16] F. Donati, S. Rusponi, S. Stepanow, C. Waeckerlin, A. Singha, L. Persichetti, R. Baltic, K. Diller, F. Patthey, E. Fernandes, J. Dreiser, Z. Sljivancanin, K. Kummer, C. Nistor, P. Gambardella, and H. Brune, Magnetic remanence in single atoms, Science **352**, 318 (2016).

[17] S. Baumann, F. Donati, S. Stepanow, S. Rusponi, W. Paul, S. Gangopadhyay, I. G. Rau, G. E. Pacchioni, L. Gragnaniello, M. Pivetta, J. Dreiser, C. Piamonteze, C. P. Lutz, R. M. Macfarlane, B. A. Jones, P. Gambardella, A. J. Heinrich, and H. Brune, Origin of perpendicular magnetic anisotropy and large orbital moment in Fe atoms on MgO, Phys. Rev. Lett. **115**, 237202 (2015).

[18] T. Schuh, T. Miyamachi, S. Gerstl, M. Geilhufe, M. Hoffmann, S. Ostanin, W. Herger, A. Ernst, and W. Wulfhekel, Magnetic excitations of rare earth atoms and clusters on metallic surfaces, Nano Lett. **12**, 4805 (2012).

[19] X. Ou, H. Wang, F. Fan, Z. Li, and H. Wu, Giant magnetic anisotropy of Co, Ru, and Os adatoms on MgO (001) surface, Phys. Rev. Lett. **115**, 257201 (2015).

[20] K. R. Meihaus and J. R. Long, Actinide-based single-molecule magnets, Dalton Trans. **44**, 2517 (2015).

[21] K. S. Pedersen, K. R. Meihaus, A. Rogalev, F. Wilhelm, D. Aravena, M. Amoza, E. Ruiz, J. R. Long, J. Bendix, and R. Clerac, $[UF_6]^{2-}$: A molecular hexafluorido actinide(IV) complex with compensating spin and orbital magnetic moments, Angew. Chem., Int. Ed. **58**, 15650 (2019).

[22] J. D. Rinehart, T. D. Harris, S. A. Kozimor, B. M. Bartlett, and J. R. Long, Magnetic exchange coupling in actinide-containing molecules, Inorg. Chem. **48**, 3382 (2009).

[23] J. Li, L. Gu, and R. Wu, Giant magnetic anisotropy energy and long coherence time of uranium substitution on defected $Al_2O_3$(0001), Phys. Rev. B **102**, 054406 (2020).

[24] W. Feng, Q. Hao, Q. Chen, R. Qiu, X. Lai, J. Chen, and Q. Liu, Comparative study of adsorptions, reactions and electronic properties of U atoms on Cu(111), Ag(111), Au(111) and Ru(0001) surfaces, Nanotechnology **32**, 425704 (2021).

[25] W. Feng, P. Yang, B. Yuan, Z. Hu, X. Zhu, Q. Hao, Y. Zhang, Q. Zhang, B. Wang, S. Tan, X. Lai, Q. Liu, and Q. Chen, Orbital selective $5f$ electron character, indication of Kondo effect, and subatomic features of single uranium atoms, Phys. Rev. B **107**, 075136 (2023).

[26] G. V. Nazin, X. H. Qiu, and W. Ho, Charging and interaction of individual impurities in a monolayer organic crystal, Phys. Rev. Lett. **95**, 166103 (2005).

[27] G. V. Nazin, X. H. Qiu, and W. Ho, Vibrational spectroscopy of individual doping centers in a monolayer organic crystal, J. Chem. Phys. **122**, 181105 (2005).

[28] B. Li, C. G. Zeng, J. Zhao, J. L. Yang, J. G. Hou, and Q. S. Zhu, Single-electron tunneling spectroscopy of single C-60 in double-barrier tunnel junction, J. Chem. Phys. **124**, 064709 (2006).

[29] G. Kresse and J. Furthmuller, Efficiency of ab-initio total energy calculations for metals and semiconductors using a plane-wave basis set, Comput. Mater. Sci. **6**, 15 (1996).

[30] P. E. Blochl, Projector augmented-wave method, Phys. Rev. B **50**, 17953 (1994).

[31] J. P. Perdew, K. Burke, and M. Ernzerhof, Generalized gradient approximation made simple, Phys. Rev. Lett. **77**, 3865 (1996).

[32] V. I. Anisimov, J. Zaanen, and O. K. Andersen, Band theory and Mott insulators: Hubbard $U$ instead of Stoner $I$, Phys. Rev. B **44**, 943 (1991).

[33] S. L. Dudarev, G. A. Botton, S. Y. Savrasov, C. J. Humphreys, and A. P. Sutton, Electron-energy-loss spectra and the structural stability of nickel oxide: An LSDA+$U$ study, Phys. Rev. B **57**, 1505 (1998).

[34] See Supplemental Material at http://link.aps.org/supplemental/10.1103/PhysRevB.108.245407 for tuning the magnetic anisotropy of single U atoms on MgO/Ag(001), which includes Refs. [26–28,35–37].

[35] S. Schintke, S. Messerli, M. Pivetta, F. Patthey, L. Libioulle, M. Stengel, A. De Vita, and W. D. Schneider, Insulator at the ultrathin limit: MgO on Ag(001), Phys. Rev. Lett. **87**, 276801 (2001).

[36] S. Baumann, I. G. Rau, S. Loth, C. P. Lutz, and A. J. Heinrich, Measuring the three-dimensional structure of ultrathin insulating films at the atomic scale, ACS Nano **8**, 1739 (2014).

[37] S. W. Chen, R. S. Ingram, M. J. Hostetler, J. J. Pietron, R. W. Murray, T. G. Schaaff, J. T. Khoury, M. M. Alvarez, and R. L. Whetten, Gold nanoelectrodes of varied size: Transition to molecule-like charging, Science **280**, 2098 (1998).

[38] M. Sterrer, T. Risse, U. M. Pozzoni, L. Giordano, M. Heyde, H.-P. Rust, G. Pacchioni, and H.-J. Freund, Control of the charge state of metal atoms on thin MgO films, Phys. Rev. Lett. **98**, 096107 (2007).

[39] M. Heyde, G. H. Simon, and L. Lichtenstein, Resolving oxide surfaces—from point and line defects to complex network structures, Phys. Status Solidi B **250**, 895 (2013).

[40] S. W. Hla, Scanning tunneling microscopy single atom/molecule manipulation and its application to nanoscience and technology, J. Vac. Sci. Technol. B **23**, 1351 (2005).

[41] D. M. Eigler and E. K. Schweizer, Positioning single atoms with a scanning tunnelling microscope, Nature (London) **344**, 524 (1990).

[42] M. Ternes, A. J. Heinrich, and W.-D. Schneider, Spectroscopic manifestations of the Kondo effect on single adatoms, J. Phys.: Condens. Matter **21**, 053001 (2009).

[43] A. A. Khajetoorians, S. Lounis, B. Chilian, A. T. Costa, L. Zhou, D. L. Mills, J. Wiebe, and R. Wiesendanger, Itinerant nature of atom-magnetization excitation by tunneling electrons, Phys. Rev. Lett. **106**, 037205 (2011).

[44] T. Balashov, M. Meyer, and W. Wulfhekel, A compact ultrahigh vacuum scanning tunneling microscope with dilution refrigeration, Rev. Sci. Instum. **89**, 113707 (2018).

[45] B. C. Stipe, M. A. Rezaei, and W. Ho, Single-molecule vibrational spectroscopy and microscopy, Science **280**, 1732 (1998).

[46] D. S. Wang, R. Q. Wu, and A. J. Freeman, First-principles theory of surface magnetocrystalline anisotropy and the diatomic-pair model, Phys. Rev. B **47**, 14932 (1993).

[47] Y. Miura, S. Ozaki, Y. Kuwahara, M. Tsujikawa, K. Abe, and M. Shirai, The origin of perpendicular magneto-crystalline anisotropy in L1(0)-FeNi under tetragonal distortion, J. Phys.: Condens. Matter **25**, 106005 (2013).